



LITHOSTRATIGRAPHY AND CHRONOLOGY OF VISTULIAN PERIGLACIAL DEPOSITS IN JÓZEFÓW (CENTRAL POLAND) BASED ON LUMINESCENCE DATING

JACEK FORYSIAK^{1,*}, ALEKSANDRA MAJECKA², PIOTR MOSKA³, LESZEK MARKS²

¹Department of Geology and Geomorphology, University of Łódź, 90-139 Łódź, Poland

²Department of Climate Geology, Faculty of Geology, University of Warsaw, 02-089 Warszawa, Poland

³Institute of Physics – Division of Geochronology and Environmental Isotopes, Institute of Physics, Silesian University of Technology, 44-100 Gliwice, Poland

Received 18 July 2023

Accepted 10 January 2024

Abstract

Sediments in Józefów were deposited in a small lake in the Eemian Interglacial and Early Vistulian (MIS 5). They were then covered by periglacial mineral sediments during the Upper Pleniglacial and the Late Vistulian (MIS 2). These sediments were deformed by gelifluction and thermokarst processes. There is no traces of deposition from MIS 4 and MIS 3. Optically stimulated luminescence (OSL) dating confirmed the age of the sediments and enabled the reconstruction of the deposition phases and deformation of the lake infilling.

Keywords

periglacial sediments, OSL dating, Upper Pleniglacial- and Late Vistulian, Polish Lowland

1. Introduction

The timing of periglacial events on the Polish Lowland is reconstructed primarily on indirect premises: (1) dating of biogenic sediments in periglacial deformations (Klatkova, 1990, 1996; Goździk, 1996; Petera, 2002), (2) the relationship between these structures and periglacial evidence to glacial phases of the last ice sheet and (3) the dating of periglacial mineral sediments (Mojski, 2005; Turkowska, 2006; Marks *et al.*, 2016).

Periglacial sediments and landforms are common in the Polish landscape and comprise slope features, river valleys, denudational plains and drainless depressions (Dylik, 1967; French, 2007). Periglacial processes transformed older landforms and created new ones. In Central Poland, there are many small buried depressions of the Saalian Glaciation

(MIS 6) age which were filled with lacustrine-terrestrial deposits during the Eemian or the Early Vistulian, covered with mineral deposits and deformed in a periglacial environment during the Last Glacial Termination (LGT).

In the second half of the 20th century, Central Poland was intensively studied and traces of the Vistulian (Weichselian) periglacial processes were identified (e.g., Dylik, 1963, 1967, 1969; Dylikowa, 1964; Goździk, 1973), including at the Józefów site. In the 1960s, research at Józefów was based primarily on the examination of periglacial features in the exposures. The age of the deposits was determined based on a pollen analysis of underlying sediments, which were correlated with the Amersfoort-Brörup interstadial (Dylik, 1969). The Józefów site consisted of four fossil depressions, in which sediments and deformation structures were identified as fragments of a

Corresponding author: J. Forysiak
e-mail: jacek.forysiak@geo.uni.lodz.pl

relict pingo (Dylik, 1963, 1967), and so far the only documented fossil pingo in Poland.

This study aimed to determine the lithostratigraphy of the Vistulian deposits supported by their sedimentological features at this site. Recently, research at Józefów has resumed in the most accessible shallow, closed basin with a dry bottom, which allowed the geological work to be performed using drillings and outcrops.

The Optically Stimulated Luminescence (OSL) method has been used successfully to date periglacial deposits at many Vistulian sites in Poland and aeolian deposits in the Polish part of the European Sand Belt: in the Silesian Lowland, the southern Mazovian Lowland and the Sandomierz Basin (Dobrowolski and Fedorowicz, 2007; Kalińska and Wyszomierski, 2010; Gębica *et al.*, 2016; Moska *et al.*, 2020, 2021b, 2023). These results show that aeolian deposits were formed during the Late Pleistocene when large ice sheets covered much of northern Europe. As the climate warmed up and the ice sheet retreated, vast amount of sand was exposed and mobilised by wind and therefore, this area is extremely interesting due to the high dynamics of changes.

Another significant area in Poland is its loess region, which allows to select the lithostratigraphic sequences spanning hundreds of thousands of years. The Polish extensive loess covers are known particularly from the central and eastern parts of the country. Loess has been widely used for optically stimulated luminescence dating (OSL; Moska *et al.*, 2012, 2015, 2017, 2019; Gębica *et al.*, 2016).

Periglacial sediments are well suited for OSL dating, but a single field reconnaissance and sampling strategy constitute a key consideration. We expect that OSL dating and lithological methods, which have not previously been applied at this site, may provide new input about the origin of sediments. This is a starting point for a more detailed approach to the recognition of processes and climatic conditions during the Vistulian, which is very diverse in terms of climatic conditions.

2. Study Site

The Józefów site (51°49'59.32"N, 19°53'24.7"E) is located on the Łódź Upland, in the third-rank watershed separating the Mroga and Jeżówka and Rawka river catchments. This area was formed primarily during the Warta Stadial of the Odranian (Saalian) Glaciation (Figs. 1A,B and Table 1) and is dominated by tills, glacial and glacio-fluvial sand and gravel (Nowacki, 1993; Trzmiel, 1994) and slope sand and silt, activated by Vistulian denudation processes.

The examined Józefów basin is amidst a dozen or so such features located on a glacial moraine plateau which is cut off from the surrounding area by denudation valleys that run westwards to the Mroga River valley and eastwards to the Rawka valley. The studied depression lies at about 200 m a.s.l., reaching to 211.5 m a.s.l and 212.7 m a.s.l. about 1 km to the south-west and north-east.

3. Material and Methods

Five outcrops were examined, two of which were partially exposed with walls of excavations made in the 1960s (sections II and V, on Fig. 2).

3.1. Lithological Analysis

Samples were collected from the same layer used for the dating. The grain-size analysis included examination of material using sieves (intervals 0.3–0.5 ϕ ; dry sieving method) (Mycielska-Dowgiałło, 1995) for each of the documented sections in outcrops (Fig. 2). Using the Folk and Ward's formula (1957), the particle coefficients were determined for each sample: mean grain diameter (Mz), sorting (σI) and skewness (SkI). Sedimentary environments were determined based on the roundness and morphoscopy of quartz grains (fraction 0.63–0.8 mm) by the modified Cailleux method (Cailleux, 1942; Klatkova, 1991; Manikowska, 1993). Five types of grains were determined: RM – round, mat (abraded in aeolian transport); EL – shiny (typical of fluvial environments); M – mediate; C – cracked (with earlier processing); NU – non-processed, fresh grains. The results are presented partially in this article, and selected samples of deposits are OSL dated (Table 1). Deposits were divided into lithofacies based on codes proposed by Zieliński (2015) (Table 2).

Sediment structures, their post-sedimentary deformations and contacts between the series were documented for all examined outcrops. Their detailed analysis will be presented in a subsequent paper.

3.2. Luminescence Dating

All samples for luminescence dating were taken from the sections with most characteristics, from a clean vertical outcrop using thin-walled steel pipes. The measurement was carried out in the Gliwice luminescence dating laboratory (Moska *et al.*, 2021a). For dose-rate determination, high-resolution gamma spectrometry was performed using a HPGe detector manufactured in Canberra in order to determine the content of U, Th and K in the sample according to the laboratory protocol (Moska *et al.*, 2021a). Dose rates were calculated using an online dose-rate calculator (Tudyka *et al.*, 2023), which contains all the latest

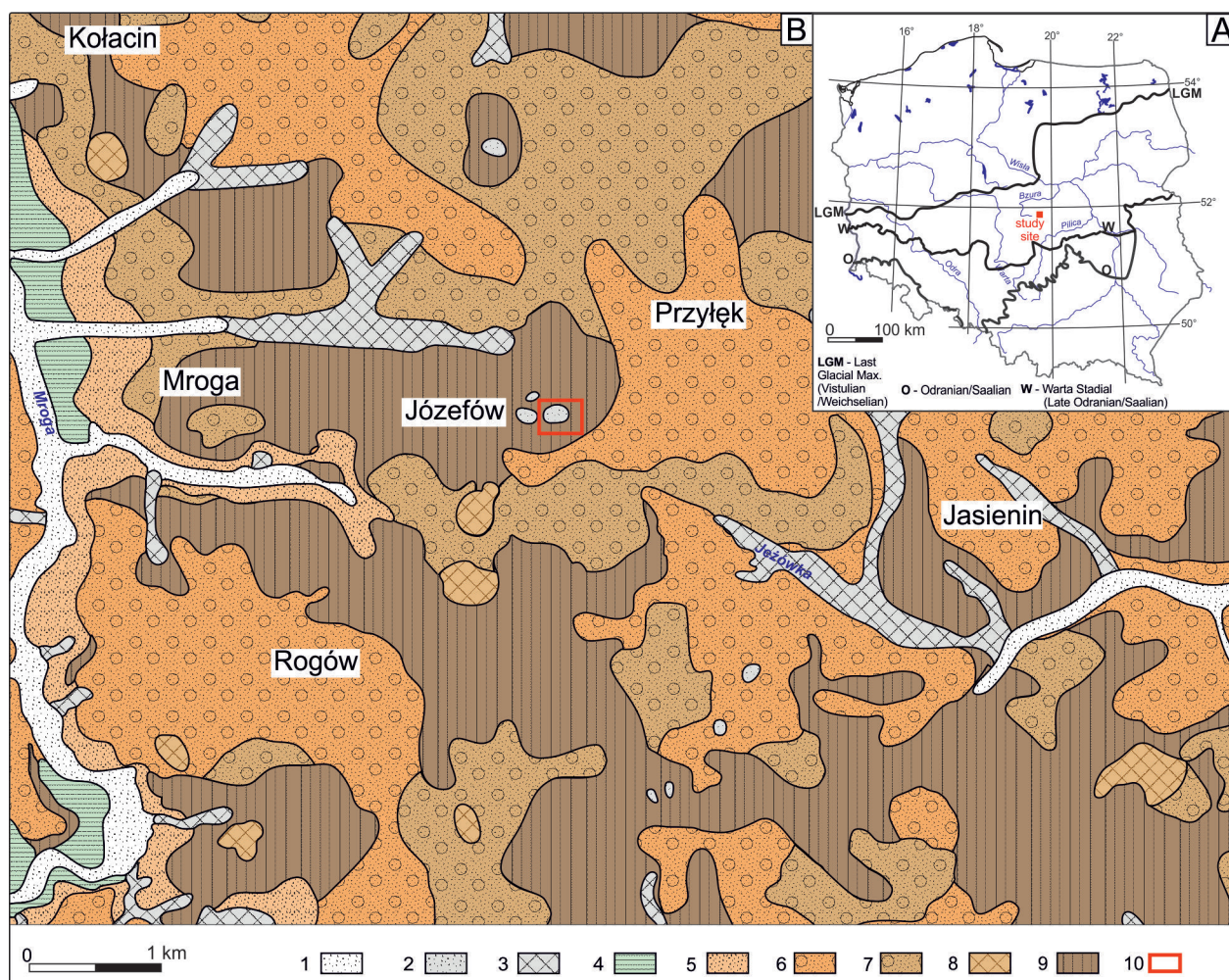


Fig 1. (A) Location of the study site in relation to extents of ice sheets, (B) Location on the geological background (according to SMGP 1:50,000). Holocene: 1 – fluvial sand and mud; Vistulian: 2 – mineral-organic mud, 3 – deluvial sand and mud, 4 – fluvial sands; Warta Stadial: 5 – glacio-fluvial sand, 6 – glaciofluvial sand and gravel, 7 – glacial sand with gravel, 8 – sand, gravel and boulder (morainic), 9 – glacial till; 10 – study site.

conversion factors. We assumed that the average water content was $15 \pm 5\%$. Data for dose-rate calculations are presented in **Table 3**.

For OSL measurements, grains of quartz (90–125 μm) were extracted from the sediment samples by routine treatment with 20% hydrochloric acid (HCl) and 20% hydrogen peroxide (H_2O_2) (Aitken, 1998). The quartz grains were sieved before they were separated using density separation with the application of sodium polytungstate solutions, leaving grains of densities between 2.62 g/cm^3 and 2.75 g/cm^3 . Finally, grains were etched with concentrated hydrofluoric acid (HF, 40 min).

All OSL measurements were performed using an automated Daybreak 2200 TL/OSL reader (Bortolot, 2000) fitted with a calibrated $^{90}\text{Sr}/^{90}\text{Y}$ beta source delivering about 2.7 Gy/min to grains at the sample position. Daybreak 2200 uses blue diodes (470 ± 4 nm)

delivering about 60 mW/cm^2 at the sample position after passing through BG39 filters. Equivalent doses were determined using the single-aliquot regenerative-dose (SAR) protocol (Murray and Wintle, 2000). The OSL SAR protocol used in our measurements comprised the following steps:

1. Irradiation with the regenerative beta dose Di
2. Preheat at 260°C for 10 s
3. Blue light stimulation at 125°C for 100 s
4. Irradiation with the test dose Dt (~10% of natural dose, but not <1 Gy)
5. Cut-heat at 220°C
6. Blue light stimulation at 125°C for 100 s

Intensities measured in steps 3 and 6 were used for equivalent dose determination. For equivalent dose

Table 1. Results of lithological analysis for most samples of deposits used for luminescence dating.

Sample ID	Ratios (ϕ)			Morphoscopy of quartz grains (%)				
	Mz	σ	Ski	RM	EL	M	C	NU
J_1	2.2	1.5	-0.5	34	10	31	19	6
J_8	2.2	0.9	0.0	39	9	38	11	3
J_9	2.1	1.2	-0.3	35	9	36	16	4
J_10	2.2	1.4	-0.3	39	11	35	13	2
J_11	3.0	1.7	0.0	37	11	30	17	5
J_12				38	6	46	8	2
J_13	1.6	2.0	-0.1	50	4	38	6	2
J_14				50	5	33	10	2
J_15	4.9	3.4	0.7					
J_16	4.4	1.8	0.5	28	18	36	15	3
J_17	2.1	1.05	-0.1	52	8	32	7	1
J_18	2.3	1.5	0.1	49	3	37	9	2
J_19	3.7	3.3	0.5	44	6	33	13	4
J_20	2.1	2.1	0.1	45	9	33	12	1
J_21	1.7	1.3	-0.1	41	10	39	9	1
J_22	1.7	1.1	-0.1	45	9	35	9	2
J_23	1.9	1.0	0.0	36	11	34	16	3
J_24	1.6	0.9	0.0	38	8	38	14	2
J_25	8.4	3.4	0.5	35	9	31	19	6

calculation, the first second of the signal was used and the background was estimated from the last 10 s.

A preheat plateau test was performed for a few samples to establish the most appropriate preheat temperature. The preheat temperatures were varied from 200°C to 300°C in 20°C steps. No systematic variation in D_e with preheat temperature was observed. Preheating the sample can also cause recuperation of the OSL signal (Aitken, 1998). To test for this, a 0 Gy regenerative dose step was added into the SAR protocol (Murray and Wintle, 2000). The luminescence signal should then be zero. Any grains for which this sensitivity-corrected recuperated signal was >5% of the corresponding natural signal should be rejected, but for all measured aliquots of investigated samples, this signal was <5%.

Final equivalent dose (D_e) values were calculated for all samples using the central age model (CAM) (Galbraith *et al.*, 1999) using the R 'Luminescence' package (Kreutzer *et al.*, 2020). All obtained luminescence results are presented in **Fig. 2**, where the D_e distributions are presented in terms of relative probability density functions (Berger, 2010). The overdispersion parameter was calculated for

each sample; these were 20% or less for all samples, so CAM was applied for final equivalent dose calculations. For an overdispersion parameter <20%, the dose distributions are usually unimodal and it can therefore be assumed that the tested material represents the well-bleached quartzes (Moska *et al.*, 2019).

4. Results

4.1. Lithological Analysis

In all outcrops, mineral deposits were distinguished as mineral and organic sediments. Eight lithofacies were distinguished in the sections. The oldest is a mineral-organic silt with sand (*FSCd*) in the central part of the basin, below 1.5 m to 2.2 m depth (section I, II, IIIa, b, **Fig. 2**). This layer is 2.5 m thick in the centre and disappears at the edge of the basin (section IIIa). In terms of grain size, these are silty-sandy sediments, with a dominant very coarse silt (28.1%). The admixture of sandy fraction is significant (29.1%), among which very fine sand (22.2%) decidedly predominates, and the admixture of organic parts reaches only 5%. The average grain diameter (Mz) is 4.9 ϕ and the sorting factor (δ) is 0.0–0.7 ϕ . At the top, there is a large share of RM (round, mat) quartz-grain processing, reaching even 37% (sample J_11, **Table 1**). All documented sections exhibit significant deformations of the *FSCd* layer, resulting from a secondary mixing of silt and sand, originally with horizontal stratification.

Overlying deposits contain much organic matter (*Cd*), resembling a peaty gyttja; the average content of organic matter is 75.9%. It lies below 1.6–2.0 m depth in the central part of the basin and is 0.2–0.4 m thick (sections I, III). In a marginal part of the basin, the layer disappears at about 1.5 m depth (section III, **Fig. 2**). This layer has strong post-sedimentary deformations and is intersected by mineral-organic silt with sand (*FSCd*), as well as contains fissures filled with sand (wedge structures) of a sandy lithofacies (*SCd*), with admixture of dispersed organic matter and broken fragments of the underlying peaty gyttja.

The sand is well or moderately well sorted with a high share of RM (round, mat) grains in quartz-grain processing, from 38% to 52% (J_8, J_12, J_17, **Table 1**). The sandy lithofacies (*SCd*) was documented only in fissure structures, open at the top of the organic lithofacies. The top part of the fissure structures is disturbed with the overlying layer and the boundary of these two lithofacies cannot be captured.

The overlying layer is composed of vari-grained sediments and varied thicknesses (sections I, II, IIIa). It is composed of sand with gravel (*SGm*) including coarse- and vari-grained sand, mostly with an admixture of gravel to a 45% or admixture of fines (3.8–15.7%). These deposits are

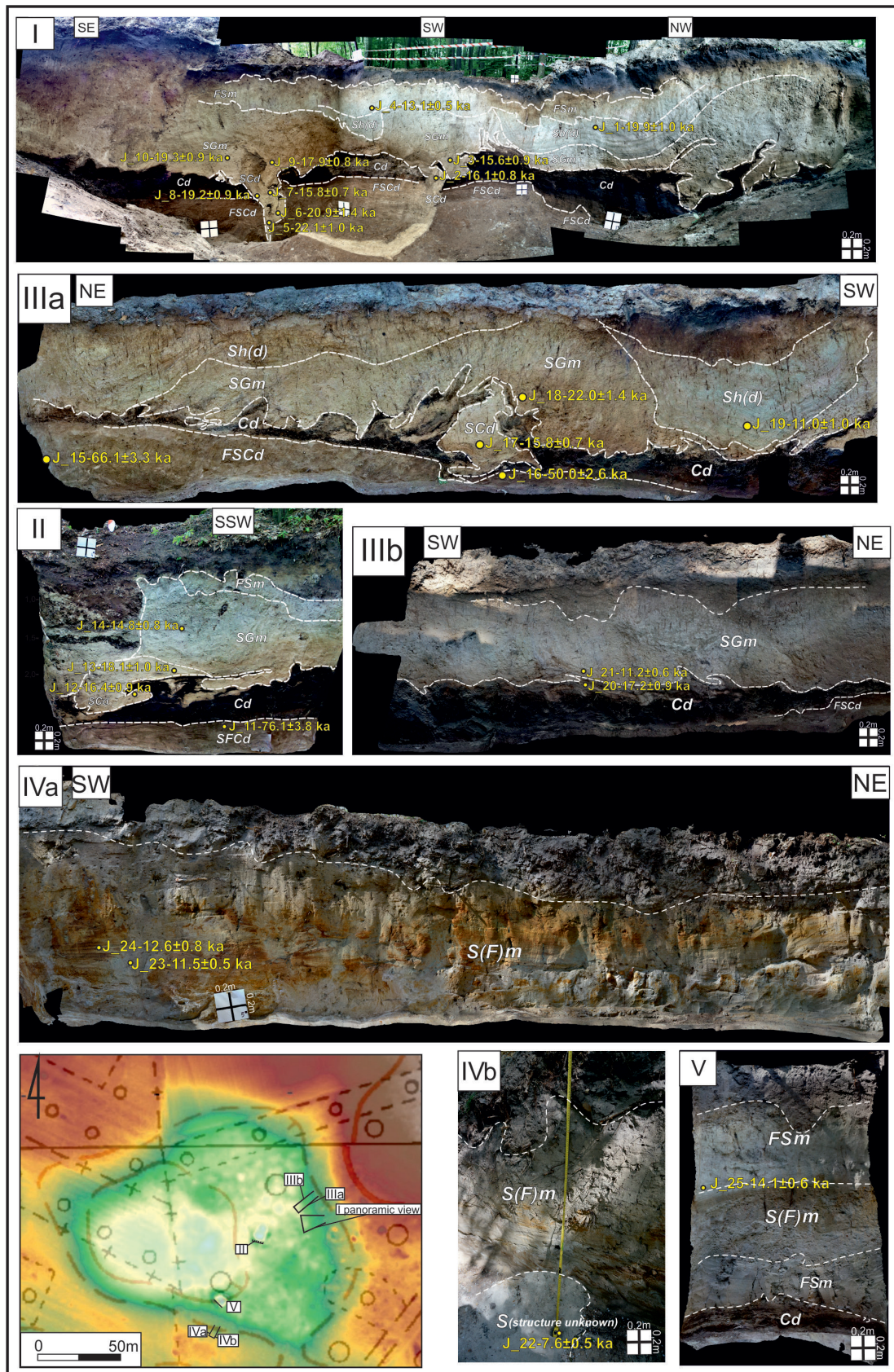


Fig 2. Orthophotomap view of the Vistulian deposits sequence in sections I-V (their location is marked on topographic sketch below) with distinguished lithofacies (Table 2) and sampling sites for luminescence dating (Table 3).

Table 2. Lithofacies code used in this study.

Code	Texture
G	Gravel
S	Sand
F	Silt
C	Organic matter
Code	Structure
<i>d</i>	Deformed
<i>m</i>	Massive
<i>h</i>	Horizontal

massive and poorly or very poorly sorted ($SD = 1.5\text{--}3.1 \phi$), but if a fine material predominates, the sorting is $1.1\text{--}1.4 \phi$. Quartz-grain processing indicated a predominance of aeolian grains ($RM = 35\text{--}49\%$) with a low share of shiny grains (EL), cracked (C) and non-processed grains (C + NU) (Table 1).

In the central part of the basin, the overlying deposits are the lacustrine sediments. They do not form a continuous layer, but they fill small basins at the top of the *SGm* lithofacies. Deformations of these deposits may result from the uneven subsidence of the basin's infilling. It is composed of sand and silt, with horizontal alternating laminae (*Sh(d)*). The laminae are not deformed, but the whole series

Table 3. All important data for investigated luminescence samples: sample names, depth, radionuclide concentration, overdispersion, dose rate, equivalent dose (CAM model) and final age.

Lab. code	Sample ID	Sample depth (cm)	Th (Bq/kg)	U (Bq/kg)	K (Bq/kg)	Dose rate (Gy/ka)	Overdispersion (%)	Equivalent dose (Gy)	OSL age (ka)
GdTL-3144	J_1	100	5.9 ± 0.2	4.7 ± 0.2	195 ± 6	0.91 ± 0.04	10	18.2 ± 0.6	19.9 ± 1.0
GdTL-3145	J_2	205	7.8 ± 0.2	5.7 ± 0.2	198 ± 6	0.93 ± 0.04	10	15.0 ± 0.5	16.1 ± 0.8
GdTL-3146	J_3	175	9.8 ± 0.2	7.9 ± 0.2	249 ± 7	1.14 ± 0.04	14	17.8 ± 0.7	15.6 ± 0.9
GdTL-3147	J_4	105	14.1 ± 0.3	12.2 ± 0.2	351 ± 10	1.59 ± 0.06	5	20.9 ± 0.5	13.1 ± 0.5
GdTL-3148	J_5	230	6.6 ± 0.2	6.2 ± 0.2	185 ± 5	0.88 ± 0.05	5	19.5 ± 0.5	22.1 ± 1.0
GdTL-3149	J_6	215	6.4 ± 0.2	6.4 ± 0.2	196 ± 6	0.91 ± 0.04	18	19.1 ± 1.0	20.9 ± 1.4
GdTL-3150	J_7	200	10.0 ± 0.2	8.1 ± 0.2	224 ± 6	1.07 ± 0.06	7	17.0 ± 0.5	15.8 ± 0.7
GdTL-3151	J_8	203	8.3 ± 0.2	7.4 ± 0.2	210 ± 6	1.00 ± 0.04	9	19.3 ± 0.6	19.2 ± 0.9
GdTL-3152	J_9	160	6.9 ± 0.2	5.8 ± 0.2	205 ± 6	0.94 ± 0.04	5	16.9 ± 0.5	17.9 ± 0.8
GdTL-3153	J_10	140	6.0 ± 0.2	5.1 ± 0.2	189 ± 5	0.88 ± 0.04	8	17.0 ± 0.5	19.3 ± 0.9
GdTL-3154	J_11	210	10.9 ± 0.3	9.3 ± 0.2	337 ± 9	1.42 ± 0.06	10	108.2 ± 3.6	76.1 ± 3.8
GdTL-3155	J_12	165	7.9 ± 0.2	7.0 ± 0.2	216 ± 6	1.01 ± 0.04	13	16.7 ± 0.7	16.4 ± 0.9
GdTL-3156	J_13	130	7.5 ± 0.2	7.6 ± 0.2	200 ± 6	0.98 ± 0.04	12	17.8 ± 0.8	18.1 ± 1.0
GdTL-3157	J_14	90	11.5 ± 0.3	10.1 ± 0.2	285 ± 8	1.34 ± 0.05	13	19.9 ± 0.8	14.8 ± 0.8
GdTL-3357	J_15	190	15.6 ± 0.3	12.8 ± 0.3	380 ± 10	1.67 ± 0.06	12	110.5 ± 3.8	66.1 ± 3.3
GdTL-3358	J_16	210	21.1 ± 0.4	18.5 ± 0.3	437 ± 11	2.00 ± 0.07	13	100.2 ± 4.2	50.0 ± 2.6
GdTL-3359	J_17	187	5.5 ± 0.2	5.0 ± 0.2	177 ± 5	0.83 ± 0.04	8	13.1 ± 0.4	15.8 ± 0.7
GdTL-3360	J_18	140	10.6 ± 0.3	9.8 ± 0.2	229 ± 7	1.16 ± 0.04	20	25.7 ± 1.3	22.0 ± 1.4
GdTL-3361	J_19	135	10.8 ± 0.3	8.8 ± 0.2	284 ± 8	1.28 ± 0.05	18	14.3 ± 0.8	11.0 ± 1.0
GdTL-3362	J_20	145	13.2 ± 0.3	12.0 ± 0.3	271 ± 8	1.33 ± 0.05	16	22.8 ± 1.0	17.2 ± 0.9
GdTL-3363	J_21	125	12.0 ± 0.3	10.2 ± 0.2	272 ± 7	1.29 ± 0.05	16	14.6 ± 0.7	11.2 ± 0.6
GdTL-3364	J_22	170	6.1 ± 0.2	5.3 ± 0.2	187 ± 6	0.87 ± 0.04	22	6.7 ± 0.4	7.6 ± 0.5
GdTL-3365	J_23	100	6.4 ± 0.2	6.2 ± 0.2	190 ± 6	0.93 ± 0.04	8	10.4 ± 0.3	11.5 ± 0.5
GdTL-3366	J_24	90	6.3 ± 0.2	5.42 ± 0.2	181 ± 5	0.89 ± 0.04	20	11.3 ± 0.6	12.6 ± 0.8
GdTL-3367	J_25	80	21.3 ± 0.5	19.2 ± 0.3	409 ± 11	1.98 ± 0.07	10	28.1 ± 0.9	14.1 ± 0.6

CAM, central age model; OSL, optically stimulated luminescence.

is co-shaped to a basin formed at the top of the underlying deposits (sections I, IIIa, **Fig. 2**). Laminae of coarse silt and fine and medium-grained sand prevails. The content of aeolian grains (RM) is varied, with most samples exhibiting a large share of them, especially in the poorly sorted layers composed of fine sand and silt. These deposits also contain a large share of mediate (M) and cracked grains (C) (J_1, J_19, **Table 1**).

The top layer at the marginal zone of the basin is composed of sediments comprising fine-grained sand with an admixture of silt (*S(F)m*) and, in the central part of the basin, silt with an admixture of sand (*FSm*). These deposits are massive but deformed, presumably resulting from soil processes (sections I, II, III, IV, V, **Fig. 2**). The quartz grains at the bottom of the layer contain strongly aeolized material, with the RM content up to 46.6%; in the upper part, it decreases to 34–38%. The sum of cracked and untreated grains remains above 20% (J_23, J_24, J_25).

The youngest OSL dated deposits were sands (*S [structure unknown]*) documented on the very southern edge of the basin (**Fig. 2**) where they occurred in the fissure infilling which, unfortunately, could not be traced as it was removed by the excavator. This deposit contained abundant aeolian grains (RM), up to 45%.

4.2. Geochronology

The luminescence dating (OSL) helped to establish a geochronology of deposits. The 25 samples tested indicate the age from 76.1 ± 3.8 ka to 7.6 ± 0.5 ka (**Table 3**). Unfortunately, deposits were subjected to post-sedimentary disturbances (**Fig. 2**) and it did not allow to construct of the age-depth model. All important data for the investigated luminescence samples are presented in the **Table 3**. The results of dating of specific lithofacies with diagrams of relative probability density functions for equivalent dose distribution are presented in **Table 4**.

5. Discussion

In the Polish Lowland, there are many fossil basins filled with biogenic deposits and mineral coverings which reflect their age and origin (e.g., Klatkova, 1989, 1990, 1996; Majecka *et al.*, 2019). Generally, deposits from closed catchments in central Poland are the source of the most complete information about the climate in the Late Pleistocene. Based on the results, a lithostratigraphic subdivision of the Vistulian deposit sequence at the Józefów site was made. Our luminescence dating of mineral deposits provides a geochronology of the events (**Fig. 3**).

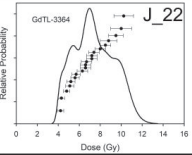
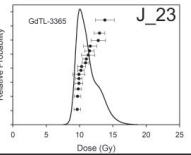
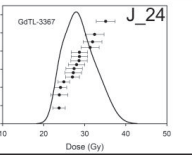
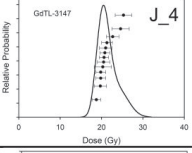
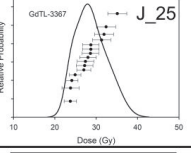
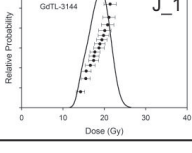
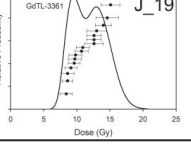
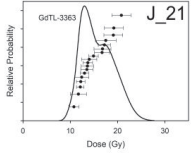
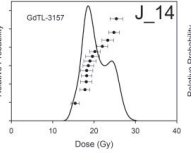
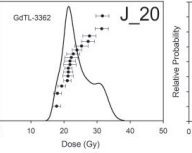
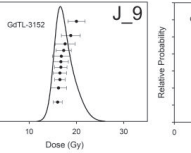
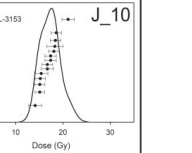
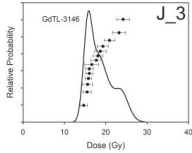
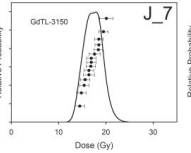
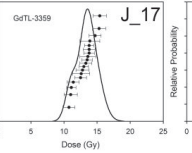
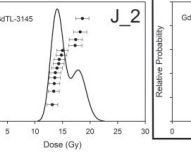
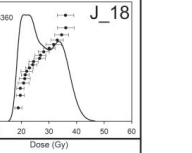
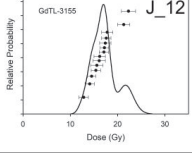
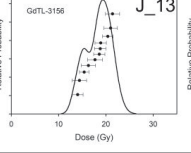
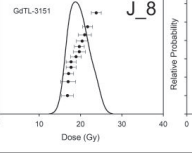
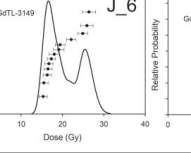
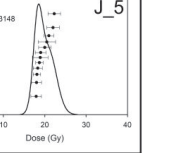
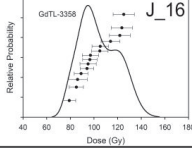
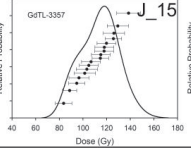
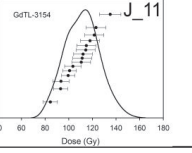
The oldest lithofacies *FSCd*, dated at 50.0–76.1 ka (GdTL-3358, GdTL-3357, GdTL-3154, **Table 2**) corresponds to the period from Early Vistulian to the Middle

Plenivistulian (Helmens, 2014; Marks *et al.*, 2016). In regional studies, such a series of sand with silt and organic material is correlated with the Early Vistulian (Klatkova, 1990, 1996). These results seem too young, but this may be due to their rejuvenation due to cryoturbation of sediments. Significant enrichment of the top part with aeolized mineral deposits proves the occurrence of aeolian processes in a cold climate during stadials of the Early Vistulian. Based on the OSL dating of this series, the overlying organic layer (*Cd*) could have been deposited during the Early Vistulian or the Middle Pleniglacial. The first option is more probable since sites with fossil soils and biogenic sediments with pleniglacial flora are generally rare in central Poland (Mamakowa, 1989; Tobolski, 1991; Balwierz, 1996; Granoszewski, 2003). There is a stratigraphic gap in central Poland covering the older part of the Plenivistulian, e.g. in the sediments of the north-western Uniejów Basin (Peters, 2002) or in valleys and closed depressions in the Łódź Upland (e.g., Klatkova, 1996).

On the assumption that the *Cd* lithofacies was deposited at the end of the Early Vistulian (MIS 5a) and the *SCd* and *SGm* lithofacies were deposited in MIS 2, as indicated by OSL dating, a period of about forty to fifty thousand years correlates with MIS 4 and 3 (Helmens, 2014; Marks *et al.*, 2016) but not represented by any deposits in the Józefów basin, similarly as in other closed depressions in central Poland (Klatkova, 1996, 1989; Majecka *et al.*, 2019).

The accumulation of the *SGm* lithofacies at the Józefów site is associated with permafrost and the deposition of gelifluctional sediments flowing down on a thawing active layer. This series is enriched with aeolian sand and it could have been blown directly into the basin or deposited on slopes and then incorporated into gelifluction deposits. The OSL ages of 17.2–22.0 ka (**Table 4**) indicate that these deposits formed concurrently with the Leszno Phase (Marks, 2012). At this time, fluvial and aeolian processes developed intensively in a periglacial cold climate in the extraglacial part of the European Lowland (Huijzer and Isarin, 1997; Vandenberghe *et al.*, 1998). The development of the Józefów basin was probably not related to fluvial processes, but certainly with aeolian and slope processes. Furthermore, a scheme of cover sand was adopted, based on the type of material and its relation to biogenic sediments and palaeosoils for the European aeolian sandy formations (Maarleveld, 1960). This scheme is referred to based on OSL dating. The Older Cover-sand I is OSL dated at 15.4–25.2 ka, but mostly at 20–22 ka in the Netherlands (Bateman and van Huissteden, 1999). The lithofacies *SGm* can therefore be correlated time-wise with this level and its deformations may have arisen during the flow of successive gelifluction lobes into the basin that were then transformed by thermokarst processes (**Fig. 2**). The two datings indicate clearly an earlier period than the others, but the

Table 4. Luminescence dating (OSL) results for documented lithofacies, with relative probability density functions for equivalent dose distribution (Berger, 2010).

Lithofacies	Sample ID	OSL age ka	Relative probability density functions for equivalent dose distribution (Berger, 2010)				
							
S S(F)m	J_22	7.6±0.5					
	J_23	11.5±0.5					
	J_24	12.6±0.8					
FSm	J_4	13.1±0.5					
	J_25	14.1±0.6					
Sh (d)	J_1	19.9±1.0					
	J_19	11.0±1.0					
SGm	J_21	11.2±0.6					
	J_14	14.8±0.8					
	J_20	17.2±0.9					
	J_9	17.9±0.8					
	J_10	19.3±0.9					
	J_18	22.0±1.4					
SCd	J_3	15.6±0.9					
	J_7	15.8±0.7					
	J_17	15.8±0.7					
	J_2	16.1±0.8					
	J_12	16.4±0.9					
	J_13	18.1±1.0					
	J_8	19.2±0.9					
	J_6	20.9±1.4					
	J_5	22.1±1.0					
	SFC d	J_16	50.0±2.6				
J_15		66.1±3.3					
J_11		76.1±3.8					

correctness of the result may be a subject to secondary rejuvenation through possible bioturbations at the site caused by the presence of burrow-forming animals like moles, foxes or badgers during the Holocene. These results were obtained from the top of the *SGm* series, which could have been subjected to post-depositional displacement closer to a topographic surface, even before the *FSm* lithofacies, and thus also exposed to rejuvenation due to exposure to daylight.

SCd lithofacies filling a fissure forms different structures which were also very important to determine the periglacial

events and their age. We did not find convincing evidence that they could belong to a polygonal system and so they are probably dilatation cracks formed due to the growth of a frost mound, the existence of which was proven earlier (Dylik, 1967). The infillings contain both well-sorted sand with abundant aeolian quartz grains and material from the *SGm* lithofacies that flowed into cracks from the immediate vicinity. Luminescence ages (Lab. Code: GdTL-3145, GdTL-3146, GdTL-3148, GdTL-3149, GdTL-3150, GdTL-3151, GdTL-3152, GdTL-3155, GdTL-3359) are dispersed from 15.6 ka to 22.1 ka (Tables 2 and 4; Fig. 2),

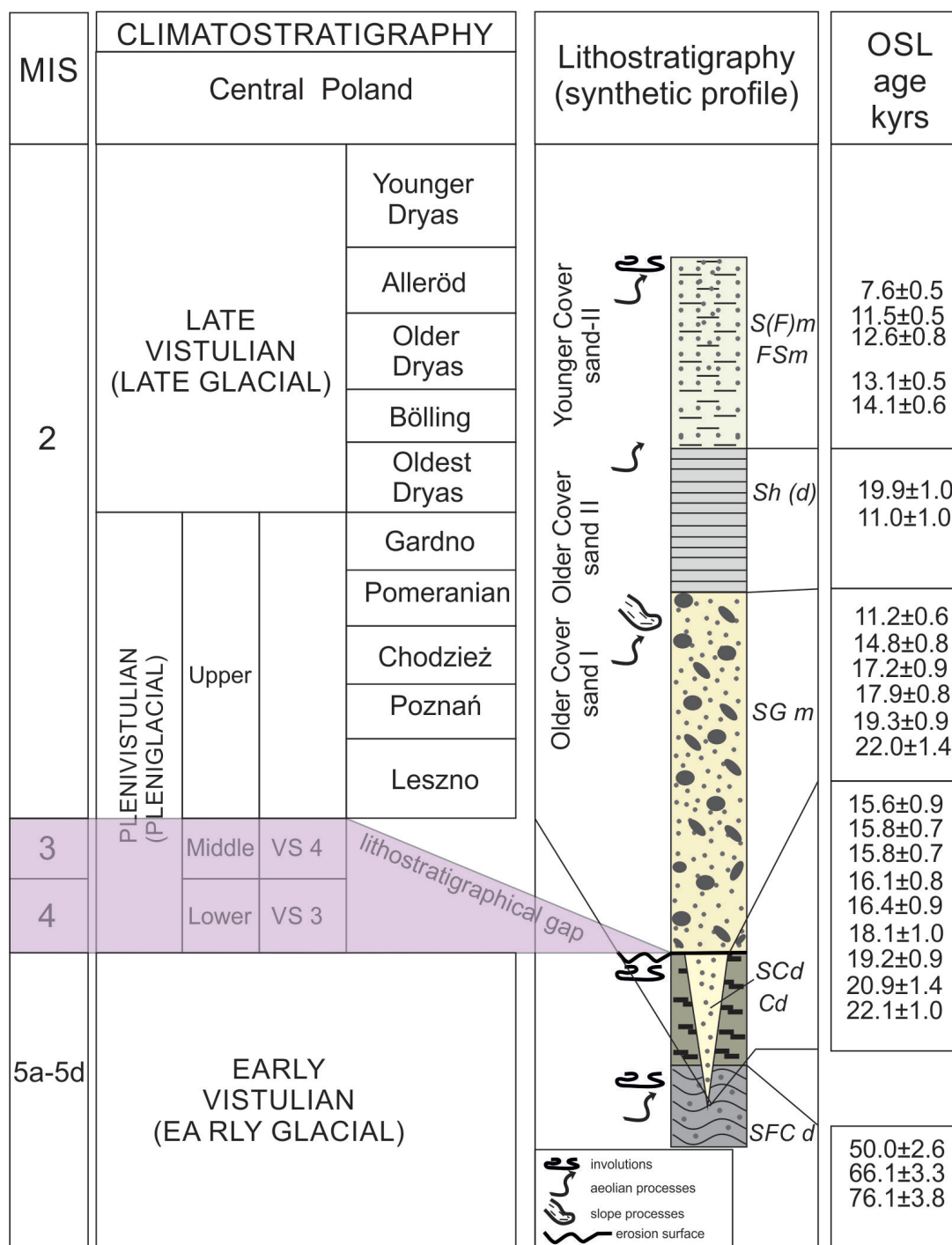


Fig 3. Lithostratigraphical scheme of the Vistulian deposits at the Józefów site with OSL age results in relationship to the Vistulian climatostratigraphy. OSL, optically stimulated luminescence.

but samples with a large amount of aeolian material are dated to about 22.0 ± 1.4 ka (J_18, **Table 1** and **Fig. 2**) and 14.8 ± 0.8 (J-14, **Table 1** and **Fig. 2**), which may indicate the time of the most harsh conditions and the development of the cracks.

The *SCd* lithofacies were deposited slightly earlier or synchronously with the deposition of the *SGm* series, and the gap fillings (dilatation or contraction structures) included both wind-provided material, which confirms a large share of RM grains or material from the immediate

surroundings, which could have already constituted the lithofacies *SGm*. The latest results may indicate the rejuvenation of the sediments, but a certain biphasic nature in the formation of the cracks and their filling cannot be ruled out.

Typically, ice-wedge structures or sand wedges have often been described in the Vistulian deposits (Kolstrup, 1986; Kasse and Vandenberghe, 1998; Murton *et al.*, 2000; Petera, 2002; French, 2007). Sand-filled wedges and patterned grounds are often OSL dated from the Late Saalian through the Middle Vistulian, but the majority of structures are dated from 22 ka to 14 ka (Briant *et al.*, 2004; Murton and Bateman, 2007; Buylaert *et al.*, 2009). Such a large time interval of changing climatic conditions makes it impossible to indicate precisely the exact event of wedge formation. The thermokarst and collapse of deposits laid down on ice were initiated by warming. In the case of the Last Glacial Maximum (LGM) ice sheet, this may have been either an interphase after the Leszno Phase dated at 24 ka or after the Poznań Phase at 19.0 ka (Marks, 2012) when the warming became more pronounced (Dzieduszyńska and Forysiak, 2019). The significance of the warming after 16.6 ka for thermokarst development is accentuated (Van Vliet-Lanoë *et al.*, 2019) and it can be correlated with the ice sheet retreat after the Pomeranian Phase (Marks, 2012). Therefore, varied OSL ages for the fillings of thermal contraction structures could be reasonably expected (Fig. 2).

The lithological features of the lithofacies *Sh(d)* indicate their deposition in small, water-filled basins and that they come from washing of fine material, but the significant share of aeolian sand grains suggests cold climate conditions. The OSL ages are too divergent (11.0–19.9 ka) so it is difficult to specify accurately the time of deposition (Table 3 and Fig. 3). In areas with aeolian and fluvio-aeolian deposition in a similar stratigraphic setting, there is the Older Cover-sand II (Kasse *et al.*, 2007). According to Bateman (2008), this layer was formed at 13.2–17.6 ka, with most ages grouped around 15 ka, which is in the Oldest Dryas (Vandenberghe *et al.*, 1998; Ammann *et al.*, 2013). The emergence of post-depositional deformations could be associated with the final thawing of buried ice during the warming at the end of the Oldest Dryas and in the Bölling. Such situations were documented in buried depressions of central Poland, where a segregation ice melting occurred, followed by a quick collapse of deposits during the Late Vistulian (Goździk and Konecka-Betley, 1992).

The upper lithofacies *F_Sm*, lying in the central part of the basin, and the slope lithofacies *S(F)m* are characterised by abundant RM grains. Two OSL ages indicate 13.1–14.1 ka (GdTL-3147, GdTL-3367) for sandy silt, which correspond to the Bölling–Alleröd and 11.5–12.6 ka (GdTL-3365, GdTL-3366, Table 3) for sandy slope deposits, which allows these sediments to be associated with the cold

climate of the Younger Dryas (Vandenberghe *et al.*, 2004; Dzieduszyńska and Forysiak, 2019). During this last cold period of the Vistulian, a discontinuous permafrost may also have been reactivated in north-western and central Europe (Petera-Zganiacz and Dzieduszyńska, 2017). In the European Lowland, deposition of aeolian sediments terminates with the Younger Cover-sand II. The fissure structure documented in section IVb on the southern slope of the basin is filled with well-sorted sand with a large proportion of RM-type quartz grains. Its age of 7.6 ± 0.5 ka (J-22, Table 3 and Fig. 2) is, like its origin, difficult to interpret because it corresponds with the Atlantic Period of the Holocene. It is possible that this is the sediment that filled the fissure, as a result of slope processes, immediately after its formation. Currently, the origin of this fissure cannot be explained. The age of 7.6 ka is highly underestimated and it is difficult to accept it from the paleogeographical point of view. This underestimation can be justified by possible bioturbations in this series.

Despite significant differences in the dating of samples collected from the same series, it seems that the OSL results confirm the temporal distribution of the depositions of successive lithofacies. It should be emphasised that dynamics of post-depositional disturbances were very high in the studied formations, so the precise matching of material packages to subsequent lithofacies has become problematic. Despite this high variability of structures, the lithostratigraphic arrangement of the series is generally confirmed by the OSL dating, which shows that, despite the high variability of sediments and the presence of post-sedimentary deformations, it is possible to reconstruct the age and sequence of events recorded in the sediments at Józefów.

6. Conclusions

The site at Józefów is very important for the regional stratigraphy of the Vistulian in the European Lowland, mainly due to the well-documented depositional succession of mineral deposits and their chronology. First of all, the depositional processes are dated here, so it supports the paleoclimatic considerations for the Vistulian. This is a period with vast climatic diversification and so difficult to unambiguously define due to different proxies obtained from different sedimentary environments. These are mostly environments that bear the hallmarks of periglacial processes, i.e. certain post-sedimentary disturbances. Therefore, another well-documented site is very important here to determine a complementary set of climatic conditions for the region.

The sequence of sediments begins with lacustrine sediments deposited during the Early Vistulian with traces of

cool intervals recorded in aeolian material delivery to the basin. The deformation structures are a record of cryogenic processes in cold climate conditions. A lack of deposits corresponds to MIS 4 and 3 and may indicate that erosion processes dominated here, but they have not been recorded in the sediments.

The accumulation of the gelifluction sandy-gravel series enriched with aeolian sand is associated with flowing down a thawed active layer in permafrost conditions during the LGM (**Fig. 3**). During the harshest climatic conditions, fissures developed and were successively filled with the inflowing gelifluction material, a thickness of which was getting increased as the supply of aeolian material increased in the cooling intervals (**Fig. 3**). During a degradation of the ice lens, small but numerous depressions were formed in the already buried basin, in which the sandy-silt deposit was probably the cause of their collapse and the

deformation of the older series lying below. It is difficult to date unambiguously these processes as they were associated with increased humidity and thus degradation of permafrost, but the content of aeolian material indicates still there are intensive aeolian processes in the region. The top series filling the depression proves that strong aeolian processes occurred in the region during the final phase of the Vistulian (Older Dryas, Younger Dryas).

Such a sedimentary record is a testimony to the thermal conditions of the Vistulian in the extraglacial zone of the Vistulian ice sheet. The gaps in the sedimentary record of the Lower and Middle Plenivistulian are specific to the region and also reflect the nature of the conditions and processes at that time.

The presented results were obtained with the support of the Polish National Science Centre, contract number: DEC-2014/15/B/ST10/03809.

References

- Aitken MJ, 1998. Introduction to optical dating, the dating of Quaternary sediments by the use of photon-stimulated luminescence. Oxford University Press, Oxford.
- Ammann B, van Raden UJ, Schwander J, Eicher U, Gilli A, Bernasconi SM, van Leeuwen JFN, Lischke H, Brooks SJ, Heiri O, Nováková K, van Hardenbroek M, von Grafenstein U, Belmecheri S, van der Knaap WO, Magny M, Eugster W, Colombaroli D, Nielsen E, Tinner W and Wright HE, 2013. Responses to rapid warming at termination 1a at Gerzensee (Central Europe): Primary succession, albedo, soils, lake development, and ecological interactions. *Palaeogeography, Palaeoclimatology, Palaeoecology* 391: 111–131.
- Balwierz Z, 1996. Vegetation of upper Vistulian cold phases in Central Poland. *Biuletyn Peryglacjalny* 34: 21–36.
- Bateman MD and van Huissteden J, 1999. The timing of last glacial periglacial and Aeolian events, twente, eastern Netherlands. *Journal of Quaternary Science* 4: 277–283.
- Bateman MD, 2008. Luminescence dating of periglacial sediments and structures. *Boreas* 37: 574–588.
- Berger GW, 2010. An alternate form of probability- distribution plot for De values. *Ancient TL* 28: 11–22.
- Bertran P, Andrieux E, Bateman M, Font M, Manchuel K and Sicilia D, 2018. Features caused by ground ice growth and decay in Late Pleistocene fluvial deposits, Paris Basin, France. *Geomorphology* 310: 84–101.
- Blaauw M and Christen JA, 2011. Flexible paleoclimate age-depth models using an autoregressive gamma process. *Bayesian Analysis* 3: 457–474.
- Bortolot VJ, 2000. A new modular high capacity OSL reader system. *Radiation Measurements* 32: 751–757.
- Briant RM, Coope GR, Preece RC, Keen DH, Boreham S, Griffiths HI, Seddon MB and Gibbard PL, 2004. Fluvial system response to Late Devensian (Weichselian) aridity, Baston, Lincolnshire, England. *Journal of Quaternary Science* 19: 479–495.
- Buylaert J-P, Ghysels G, Murray AS, Thomsen KJ, Vandenberghe D, DE Corte F, Heyse I and Van Den Haute P, 2009. Optical dating of relict sand wedges and composite-wedge pseudomorphs in Flanders, Belgium. *Boreas* 38: 160–175.
- Cailleux A, 1942. Les actions eoliennes periglaciares en Europe. *Mémoires de la Société Géologique de France* 46: 1–176.
- Dobrowolski R and Fedorowicz S, 2007. Glacial and periglacial transformation of palaeokarst in the Lublin–Volhynia region (SE Poland, NW Ukraine) on the base of TL dating. *Geochronometria* 27: 41–46.
- Dylik J, 1963. Traces of thermokarst in the Pleistocene sediments of Poland. *Bulletin de la Société des Sciences et des Lettres de Łódź* 14: 1–16.
- Dylik J, 1967. Główne elementy paleogeografii młodszego plejstocenu Polski Środkowej. In: Galon R and Dylik J, eds., *Czwartorzęd Polski*. Państwowe Wydawnictwo Naukowe, Warszawa: 311–352.
- Dylik J, 1969. Najstarszy interstadiał ostatniego pietra zimnego w Polsce (amersfoort). *Geological Quarterly* 13: 408–423.
- Dylikowa A, 1964. Structures de pression congélistatiques et structures de gonflement par le gel près de Katarzynow, près de Lodz. *Bulletin de la Société des Lettres de Lodz* 12(9): 1–19.
- Dzieduszyńska D and Forsytek J, 2019. Chronostratigraphy of the late Vistulian in central Poland and the correlation with Vistulian glacial phases. *Studia Quaternaria* 36(2): 137–145.
- Forsytek J, Majecka A, Marks L and Okupny D, 2018. Eemian to Early Weichselian organic deposits in the watershed kettle-hole basins in central Poland. *Bulletin of the Geological Society of Finland* 90: 199–208.

- French HM, 2007. *The Periglacial Environment*. Wiley, London.
- Galbraith R, Roberts R, Laslett G, Yoshida H and Olley J, 1999. Optical dating of single and multiple grains of quartz from jinnium rock shelter, northern Australia: Part I. experimental design and statistical models. *Journal of Archaeometry* 41: 339–364. DOI 10.1111/j.1475-4754.1999.tb00988.x.
- Gębica P, Bluszcz A and Woronko B, 2016. Origin and age of dune in the Dąbrówki village (Sandomierz Basin, Wisłok valley) in the light of lithological analysis of sediments and OSL dating. In: Święchowicz J and Michno A, eds., *Wybrane zagadnienia geomorfologii eolicznej*, Institute of Geography and Spatial Management, Jagiellonian University, Kraków: 305–330.
- Goździk J, 1973. Origin and stratigraphical position of periglacial structures in Middle Poland. *Acta Geographica Lodziensia* 31: 1–117.
- Goździk JS, 1996. A permafrost evolution and its impact on some depositional conditions between 20 and 10 ka in Poland. *Biuletyn Peryglacjalny* 34: 53–72.
- Goździk JS and Konecka-Betley K, 1992. Późnowistuliańskie utwory węglanowe w zagłębieniach bezodpływowych rejonu kopalni Bełchatów. Cz. I. Geneza i stratygrafia. *Roczniki Gleboznawcze* 43(3–4): 103–112.
- Granoszewski W, 2003. Late Pleistocene vegetation history and climatic changes at Horoszki Duże, eastern Poland: A palaeobotanical study. *Acta Palaeobotanica* 4(Suppl): 3–95.
- Helmens KF, 2014. The Last Interglacial-Glacial cycle (MIS 5-2) re-examined based on long proxy records from central and northern Europe. *Quaternary Science Reviews* 86: 115–143.
- Huijzer AS and Isarin RFB, 1997. The reconstruction of past climates using multiproxy evidence; an example of the Weichselian Pleniglacial in north-west and central Europe. *Quaternary Science Reviews* 16: 513–533.
- IAEA/RL/148, 1987. Technical Report. International Atomic Energy Agency, Vienna.
- Kalińska E and Wyszomierski M, 2010. Nowe dane odnośnie genezy i wieku form stożkopodobnych południowej części Niziny Środkowomazowieckiej. *Landform Analysis* 13: 27–31.
- Kasse C and Vandenberghe J, 1998. Topographic and drainage control on Weichselian icewedge and sand-wedge formation, Vennebrügge, German-Dutch Border. *Permafrost Periglacial Process* 9: 95–106.
- Kasse C, Vandenberghe D, de Corte F and van den Haute P, 2007. Late Weichselian fluvio-aeolian sands and coversands of the type locality Grubbenvorst (southern Netherlands): Sedimentary environments, climate record and age. *Journal of Quaternary Science* 22: 695–708.
- Klatkova H, 1989. The incorporation of closed depression into the open erosional system as one of the models of head valley stretch fashioning in the Vistulian. *Quaestiones Geographicae* 2: 83–91.
- Klatkova H, 1990. Występowanie eemskich osadów organicznych i uwagi o paleomorfologii środkowej Polski u schyłku warty i podczas eemu. *Acta Geographica Lodziensia* 61: 7–18.
- Klatkova H, 1991. Wyniki analizy morfoskopowej wybranych osadów czwartorzędowych środkowej Polski. In: Kostrzewski A., (ed.), *Geneza, litologia i stratygrafia utworów czwartorzędowych*. Poznań, Wydawnictwo UAM, Ser. Geografia; 50
- Klatkova H, 1996. Symptoms of the permafrost presence in middle Poland during the last 150 000 years. *Biuletyn Peryglacjalny* 35: 45–72.
- Kolstrup E, 1986. Reappraisal of the upper Weichselian periglacial environment from Danish frost wedge casts. *Palaeogeography, Palaeoclimatology, Palaeoecology* 56: 237–249.
- Kreutzer S, Burow C, Dietze M, Fuchs M, Schmidt C, Fischer M, Friedrich J, Riedesel S, Autzen M and Mittelstrass D, 2020. Luminescence: Comprehensive luminescence dating data analysis. R package version 0.9.10. WEB site: <<https://CRAN.R-project.org/package=Luminescence>>. Accessed 2021 July 28.
- Maarleveld GC, 1960. Wind directions and cover sands in the Netherlands. *Biuletyn Peryglacjalny* 8: 49–58.
- Majecka A, Forysiak J, Marks L and Tołoczko-Pasek A, 2019. Lithological diversity of the deposits of closed depressions in Central Poland as a result of their origin conditions. *Quaternary International* 501: 208–218.
- Mamakowa K, 1989. Late middle polish glaciation, Eemian and early Vistulian vegetation at Imbramowice near Wrocław and the pollen stratigraphy of this part of the Pleistocene in Poland. *Acta Palaeobotanica* 29(1): 11–176.
- Manikowska B, 1993. Mineralogy and abrasion of sands grains due to Vistulian (Late Pleistocene) Aeolian process in Central Poland. *Geologie en Mijnbouw* 72: 167–177.
- Marks L, 2012. Timing of the Late Vistulian (Weichselian) glacial phases in Poland. *Quaternary Science Reviews* 44: 81–88.
- Marks L, Gałązka D and Woronko B, 2016. Climate, environment and stratigraphy of the Pleistocene last glacial stage in Poland. *Quaternary International* 420: 259–271.
- Mojski JE, 2005. Ziemia polskie w czwartorzędzie. Zarys morfogenezy. PIG, Warszawa, Poland.
- Moska P and Bluszcz A, 2013. Luminescence dating of loess profiles in Poland. *Quaternary International* 296: 51–60.
- Moska P, Adamiec G and Jary Z, 2012. High resolution dating of loess profile from Biały Kościół, southwest Poland. *Quaternary Geochronology* 10: 87–93, DOI 10.1016/j.quageo.0.04.003.
- Moska P, Adamiec G, Jary Z and Bluszcz A, 2017. OSL chronostratigraphy for loess deposits from Tyszowce – Poland. *Geochronometria* 44: 307–318, DOI 10.1515/geochr-2015-0074.
- Moska P, Bluszcz A, Poręba G, Tudyka K, Adamiec G, Szymak A and Przybyła A, 2021a. Luminescence dating procedures at Gliwice luminescence dating laboratory. *Geochronometria* 48: 1–15.
- Moska P, Sokołowski RJ, Jary Z, Zieliński P, Raczek J, Szymak A, Krawczyk M, Skurzyński J, Poręba G, Łopuch M and Tudyka K, 2021b. Stratigraphy of the Late Glacial and Holocene Aeolian series in different sedimentary zones related to the Last

- Glacial maximum in Poland. *Quaternary International*, DOI 10.1016/j.quaint.04.004.
- Moska P, Jary Z, Adamiec G and Bluszcz A, 2015. OSL chronostratigraphy of a loess-paleosol sequence in Złota using quartz and polymineral fine grains. *Radiation Measurements* 81: 23–31.
- Moska P, Jary Z, Adamiec G and Bluszcz A, 2019. Chronostratigraphy of a loess-paleosol sequence in Biały Kościół, Poland using OSL and radiocarbon dating. *Quaternary International* 502: 4–17, DOI 10.1016/j.quaint.2018.05.024.
- Moska P, Jary Z, Sokołowski RJ, Poręba G, Raczyk J, Krawczyk M, Skurzyński J, Zieliński P, Michczyński A, Tudyka K, Adamiec G, Piotrowska N, Pawełczyk F, Łopuch M, Szymak A and Ryzner K, 2020. Chronostratigraphy of late glacial aeolian activity in SW Poland – a case study from the Niemodlin Plateau. *Geochronometria* 47: 124–137.
- Moska P, Sokołowski RJ, Zieliński P, Jary Z, Raczyk J, Mroczek P, Szymak A, Krawczyk M, Skurzyński J, Poręba G and Łopuch Tudyka K, 2023. An impact of short-term climate oscillations in the Late Pleniglacial and Late Glacial on sedimentary processes and the Pedogenic record in central Poland. *Annals of the American Association of Geographers* 113: 46–70.
- Murray AS and Wintle AG, 2000. Luminescence dating of quartz using an improved single-aliquot regenerative-dose protocol. *Radiation Measurements* 32(1): 57–73, DOI 10.1016/S1350-4487(99)00253-X.
- Murton B, Worsley P and Goździk J, 2000. Sand veins and wedges in cold Aeolian environments. *Quaternary Science Reviews* 19: 899–922.
- Murton JB and Bateman MD, 2007. Syngenetic sand veins and anti-syngenetic sand wedges, Tuktoyaktuk Coastlands, western Arctic Canada. *Permafrost and Periglacial Processes* 18: 33–47.
- Mycielska-Dowgiało E, 1995. Wybrane cechy teksturalne osadów [Some textural features of deposits and their significance for interpretations]. In: Mycielska-Dowgiało E and Rutkowski J, eds., *Badania osadów czwartorzędowych. Wybrane metody i interpretacja wyników [Investigations of Quaternary sediments. Some method sand interpretation of the results]*. University of Warsaw, Warszawa, Poland: 29–105.
- Nowacki K, 1993. Szczegółowa mapa geologiczna Polski 1:50 000 (Detailed geological map of Poland, Łyszkowice sheet). PIG, Warszawa.
- Petera J, 2002. Vistulian valley deposits in the Uniejów Basin and their palaeogeographical significance. *Acta Geographica Lodziensia* 83: 1–174.
- Petera-Zganiacz J and Dzieduszyńska DA, 2017. Palaeoenvironmental proxies for permafrost presence during the younger dryas, Central Poland. *Permafrost and Periglacial Processes* 28: 726–740.
- Tobolski K, 1991. Biostratigraphy and palaeoecology of the Eemian Inter glacial and the Vistulian Glaciation of the Konin region. In: *Przemiany środowiska geograficznego obszaru Konin-Turek* (ed. W. Stankowski): 45–87. UAM, Poznań
- Trzmiel B, 1994. Szczegółowa Mapa Geologiczna Polski (Detailed geological map of Poland, Brzeziny sheet). PIG BIP Warszawa.
- Tudyka K, Koruszowicz M, Osadnik R, Adamiec G, Moska P, Szymak A, Bluszcz A, Zhang J, Kolb T and Poręba G, 2023. μ Rate: An online dose rate calculator for trapped charge dating. *Archaeometry* 65: 423–443, DOI 10.1111/arc.12828.
- Turkowska K, 2006. *Geomorfologia regionu łódzkiego*. University of Lodz Press, Łódź, Poland.
- Van Vliet-Lanoë B, Pissart A, Baize S, Brulhet J and Ego F, 2019. Evidence of multiple thermokarst events in north-eastern France and southern Belgium during the two last glaciations. A discussion on 'Features caused by ground ice growth and decay in Late Pleistocene fluvial deposits, Paris basin, France' (Bertran et al., 2018). *Geomorphology* 327: 613–628.
- Vandenbergh D, Kasse C, Hossain SM, De Corte F, Van Den Haute P, Fuchs M and Murray As, 2004. Exploring the method of optical dating and comparison of optical and C-14 ages of Late Weichselian coversands in the southern Netherlands. *Journal of Quaternary Science* 19: 73–86.
- Vandenbergh J, Coope R and Kasse K, 1998. Quantitative reconstructions of palaeoclimates during the last interglacial-glacial in western and central Europe: An introduction. *Journal of Quaternary Science* 13(5): 361–366.
- Zieliński T, 2015. *Sedymentology. Deposits of rivers and lakes*. Scientific Publishers of UAM, Poznań, Poland.